Progress In Electromagnetics Research C, Vol. 127, 263–277, 2022

Compact, Gain-Enhanced, Linearly Tapered Slot Antenna with a Combined Director Using a Strip Director and Double-Sided Metamaterial Loading for UWB Applications

Junho Yeo*

Abstract—A compact, gain-enhanced, linearly tapered slot antenna (LTSA) with hook-shaped slots in the ground plane and a combined director, consisting of a metallic strip director and double-sided metamaterial (DS-MTM) loading surrounding it, is proposed for ultra-wideband (UWB) applications. Hook-shaped slots are appended in the ground plane for miniaturization, whereas a combination of the metallic strip and DS-MTM loading placed above the LTSA is used for gain enhancement. Performance of the proposed combined director is compared with other commonly used director configurations in the literature, such as single strip director, two strip directors, and two-layers of DS-MTM. It was found that gain enhancement effect of the proposed combined director is greater over the UWB than other director configurations. The fabricated prototype of the proposed antenna operates from 2.83 GHz to 11.31 GHz (119.9%) for a voltage standing wave ratio less than 2 with moderate gain of 3.2–7.5 dBi. The dimensions of the proposed LTSA in terms of the free space wavelength at the lowest frequency (λ_0) are $0.28\lambda_0 \times 0.30\lambda_0 \times 0.0075\lambda_0$ (30 mm × 32 mm × 0.8 mm), which are very compact.

1. INTRODUCTION

Ultra-wideband (UWB) technology uses a very low power short pulse for short-range, high-speed data rate, and wide bandwidth communications. It has been widely used for real-time location, radar, and imaging systems after the release of the regulation in the frequencies between 3.1 and 10.6 GHz by the United States Federal Communication Commission in 2002 [1].

Wideband antennas with broad impedance bandwidth and stable radiation patterns are required for UWB applications [2]. UWB antennas can be classified into omnidirectional and directional according to the shape of the radiation patterns. Monopole, dipole, slot, conical, and loop antennas belong to omnidirectional antennas, whereas spiral, horn, and log-periodic dipole array antennas are directional antennas [3].

Among various UWB directional antennas, tapered slot antennas (TSAs) have been widely used because of their advantages such as low profile, wide bandwidth, high gain, and good directivity. The concept of the TSAs was first introduced as flared slots in the late 1950s [4], and they had been extensively investigated after Gibson developed the Vivaldi antenna [5], which is considered as the first exponential TSA with symmetric E- and H-plane beamwidths. The tapered slot is wide at the outer end and tapers inwardly to meet a narrow slot line. There exist different types of TSAs depending on the shape of the tapered slot, such as linear, exponential (Vivaldi), constant width, elliptical, or dual exponential [6].

For UWB applications such as radar or imaging systems, compact wideband directional antennas with enhanced gain characteristic are required. Miniaturization of the TSAs can be achieved by using

Received 28 October 2022, Accepted 14 December 2022, Scheduled 22 December 2022
* Corresponding author: Junho Yeo (jyeo@daegu.ac.kr).
The author is with the School of Artificial Intelligence, Daegu University, Jillyang, Gyeongsan, Gyeongbuk 38453, Korea.

a modified tapered slot structure, a modification of the sides of the tapered slot by inserting slots with different shapes such as quarter circular, eye, exponential, or semi-circular arc, or an optimized feed transition. A compact-size asymmetrical linearly tapered slot antenna (LTSA) was introduced for portable UWB imaging systems [7]. A triangular slot was etched on the left side, and corrugated patterns were added on the right side for size reduction. A compact elliptically TSA fed by a coplanar waveguide with a pair of quarter circular slots and nonuniform corrugation was proposed for UWB applications [8]. Two pairs of eye-shaped slots were appended in order to reduce the size of the Vivaldi antenna [9]. A miniaturized UWB dual-layered Vivaldi antenna with two radiating patches and pairs of symmetrical exponential slots was reported [10]. A semi-circular patch-embedded Vivaldi antenna was proposed for miniaturized UWB radar sensors [11]. Two exponential arms were employed for the miniaturization of the UWB antipodal TSA [12]. Two exponential strip arms can be considered as the modification of the sides for the tapered slot. A compact UWB Vivaldi TSA with optimized microstrip to slotline transition was introduced for UWB applications [13].

To enhance gain characteristic of UWB TSAs, a parasitic metallic patch, a dielectric lens/cover, or a metamaterial loading/lens using periodic unit cells has been applied as a director. First, for gain improvement using a parasitic metallic patch, an elliptical patch [14, 15], a diamond-shaped metallic director [16], or three metallic coupling strips [17] were inserted inside the aperture of the tapered slot or protruded forward in some cases.

Second, in the case of using a dielectric lens or cover for the enhancement of gain, a dielectric inclusion with high dielectric constant materials in the tapered slot aperture or a dielectric lens with different shapes placed above the tapered slot was used. A profiled piece of a higher dielectric constant material was inserted in the aperture of a balanced antipodal Vivaldi antenna as a wave-guiding director to improve the antenna directivity [18]. A half-elliptical-shape [19, 20] or a trapezoidal-shape [21] dielectric lens was appended above the tapered slot of the antipodal Vivaldi antenna. An exponential-shape dielectric lens with a higher dielectric constant material was included in part of the substrate in the antenna aperture [22]. A multi-layer dielectric lens consisting of two fan-shaped dielectrics and a half-circular-shaped dielectric with different dielectric constants was included in the aperture of the tapered slot [23]. Two dielectric sheets with elliptically elongated profiles were placed above and below the TSA with some air spacing as a cover [24].

Third, artificial materials consisting of periodic structures, called metamaterials (MTMs), were applied to the aperture of the tapered slot or above it to enhance the TSA's gain. MTMs can be classified as resonant and non-resonant depending on the frequency characteristics of extracted equivalent permittivity and permeability of MTMs. For the cases of using resonant MTMs, anisotropic zero-index or index-near-zero MTMs using a meander-line [25–27] or a modified split ring [28, 29] unit cell were used. However, the frequency band for gain enhancement is limited to narrow band because of the resonant characteristic of the unit cell. In order to increase the bandwidth of gain enhancement, non-resonant MTMs using a modified parallel line [30] or rectangular patch [31] unit cell were used. MTM slabs consisting of a modified parallel line structure were applied as covers of the antipodal Vivaldi antenna in order to reduce the thickness of the slabs, cost, and weight [32].

In this paper, the design of a compact, gain-enhanced, linearly TSA (LTSA) with a combined director using a single metallic strip and double-sided MTM (DS-MTM) loading for UWB applications is presented to cover the 3.1 GHz to 10.6 GHz UWB frequency. In order to decrease the size of the reference LTSA, hook-shaped slots were inserted in the ground plane of the LTSA [3]. Next, a strip director and an array of non-resonant DS-MTM surrounding the director were employed in turn to increase antenna gain [30]. The performance, such as input reflection coefficient, radiation pattern, electric-field distribution, and gain, of the proposed LTSA with the hook-shaped slots and the combined director was compared with other cases when hook-shaped slots, a strip director, and surrounding DS-MTM loading are added one by one from the reference LTSA. In addition, the performance was compared with the cases of two strip directors and two layers of DS-MTM loading. CST Studio Suite was used for all the simulations in the paper [33].

2. ANTENNA GEOMETRY AND DESIGN PROCEDURE

The geometries of the proposed LTSA along with the unit cell dimensions of the DS-MTM are shown in Figure 1. On top of a substrate, a ground plane with a linearly tapered slot terminates with a circular slot, and hook-shaped slots, a strip director, and an arrays of DS-MTM surrounding it are printed. The unit cell of DS-MTM consists of an array of eight thin strips printed on the top and bottom sides of the substrate. The dimensions of the DS-MTM are designed to operate in non-resonant region to cover the UWB frequency band. A microstrip feed line comprising a circular stub with a two-step bent transmission line is printed on the bottom. A layer of double-sided metamaterials is also printed on the bottom. The proposed LTSA is designed using an FR4 substrate, which has a dielectric constant of 4.4 and a thickness of $h = 0.8$ mm (loss tangent = 0.025). The length and width of the substrate are $L = 32$ mm and $W = 30$ mm, respectively. The final design parameters of the proposed antenna are listed in Table 1.

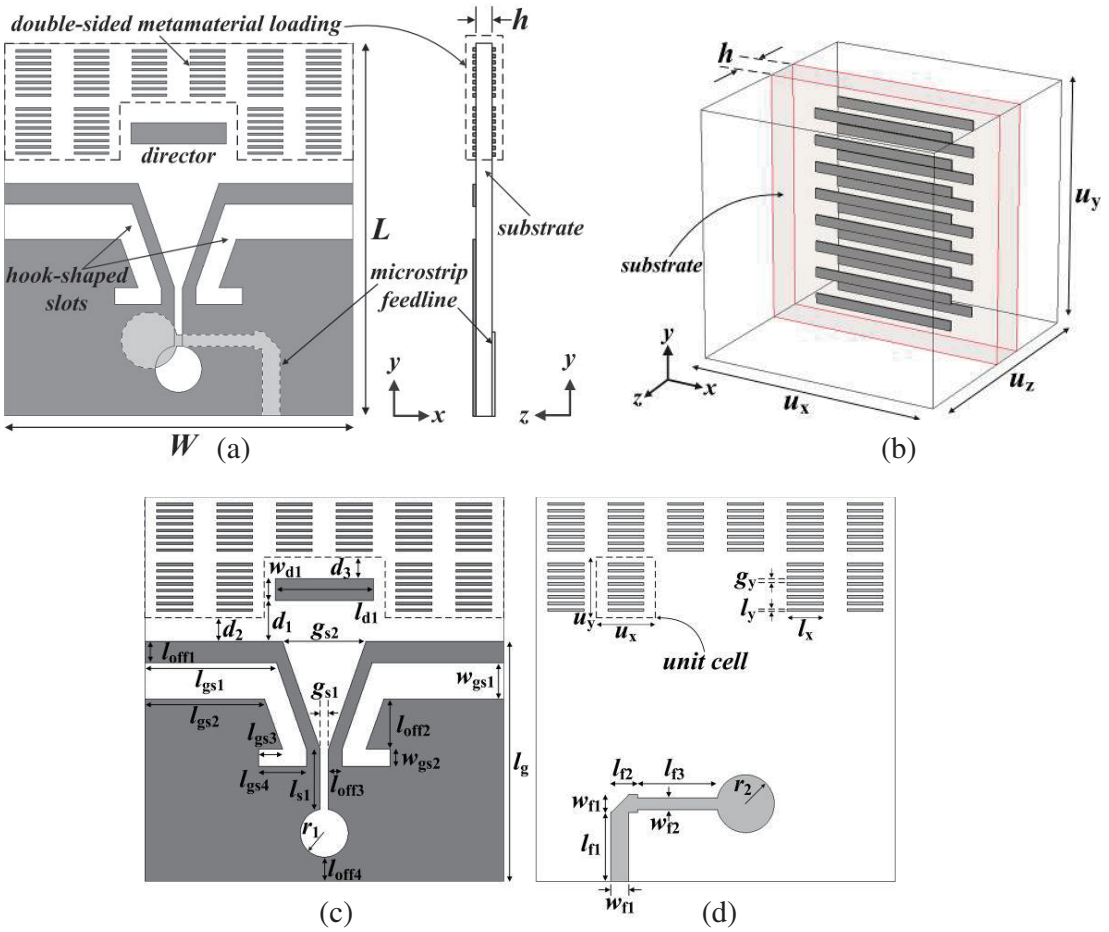

Figure 1. Geometries and surface current distributions of proposed antenna: (a) top and side views, (b) a unit cell of the DS-MTM, (c) top view only, and (d) bottom view only.

Configurations of various LTSAs examined during the design process are shown in Figure 2. Figure 2(a) shows the reference LTSA, and Figure 2(b) shows the LTSA with hook-shaped slots. Figure 2(c) is an LTSA with hook-shaped slots and one director, whereas Figure 2(d) is an LTSA with hook-shaped slots and two directors [3]. Figure 2(e) is an LTSA with hook-shaped slots and two layers of DS-MTM. The proposed LTSA with hook-shaped slots, one director, and DS-MTM is shown in Figure 2(f).

The input reflection coefficient and gain characteristics of the six antenna configurations are

Table 1. Final geometric parameters of the proposed antenna.

Parameters	Value (mm)	Parameters	Value (mm)
d_1	3.4	g_{s2}	13.5
d_2	2.5	w_{gs1}	3
d_3	2.3	w_{gs2}	1.4
l_{d1}	8.2	r_1	4
w_{d1}	1.8	r_2	4.8
l_g	20	l_{f1}	6.2
l_{off1}	1.8	l_{f2}	2.25
l_{off2}	4.6	l_{f3}	6.6
l_{off3}	1.5	w_{f1}	1.54
l_{off4}	2	w_{f2}	1.1
l_{gs1}	11	u_x	5
l_{gs2}	10	u_y	5
l_{gs3}	2	u_z	5
l_{gs4}	4	l_x	3
l_{s1}	5.03	l_y	0.2
g_{s1}	0.7	g_y	0.34

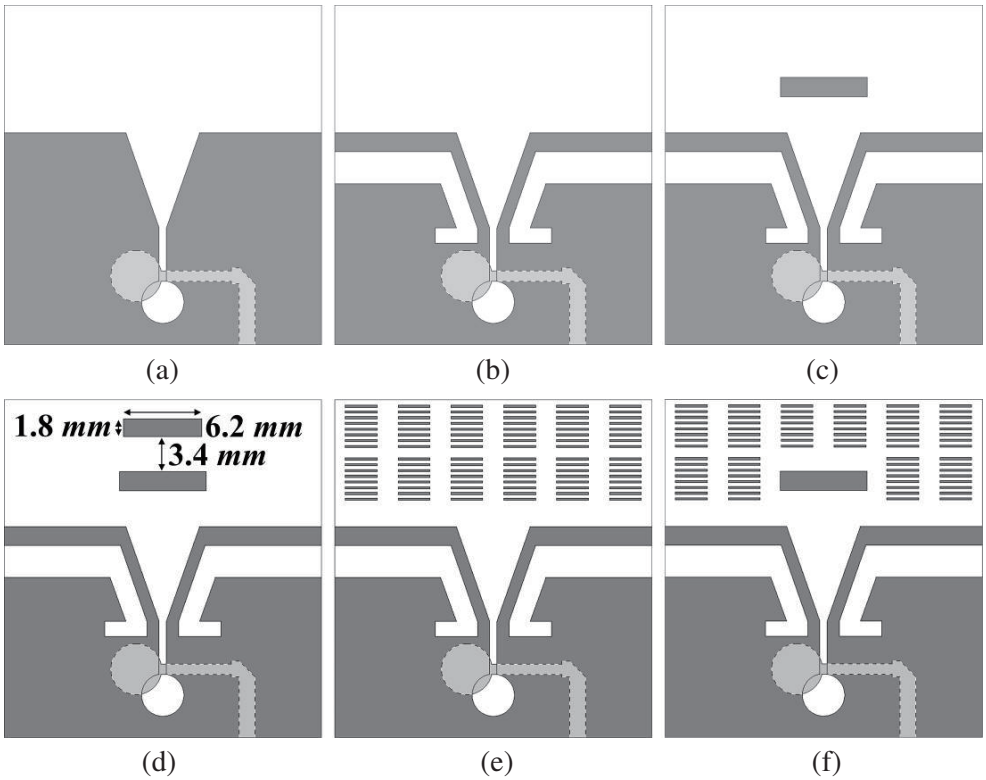

Figure 2. Antenna configurations considered for the design procedure: (a) the reference LTSA, (b) an LTSA with hook-shaped slots, (c) an LTSA with hook-shaped slots and one director, (d) an LTSA with hook-shaped slots and two directors, (e) an LTSA with hook-shaped slots and two-layer DS-MTM, and (f) the proposed LTSA with hook-shaped slots, one director, and DS-MTM.

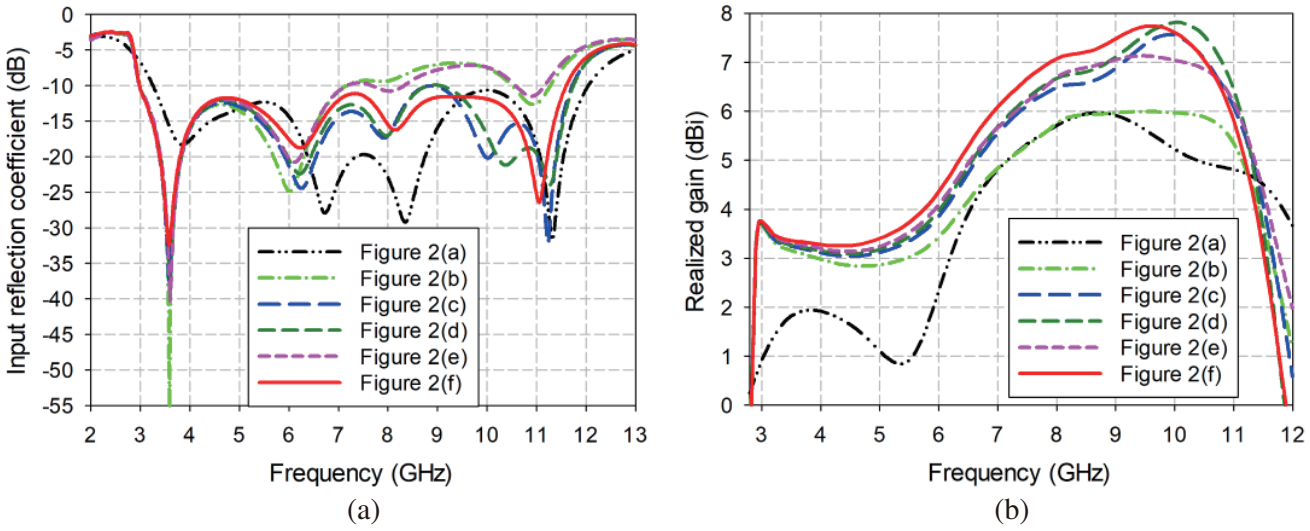

Figure 3. Performance comparison of the antennas in Figure 2. (a) input reflection coefficient and (b) realized gain.

simulated, as shown in Figure 3. For the reference LTSA shown in Figure 2(a), the frequency band for a voltage standing wave ratio (VSWR) < 2 is 3.22 GHz to 12.10 GHz (115.9%), and the lower frequency limit does not satisfy the UWB (3.1 GHz to 10.6 GHz). Gain in the UWB is 0.8–6.3 dBi. The slot opening width g_{s2} of the reference LTSA was calculated by using the following equation [34]:

$$g_{s2} = \frac{c}{f_{\max}\sqrt{\varepsilon_r}} \tag{1}$$

where c is the speed of light; ε_r is the relative permittivity of the substrate; and $f_{\max}$ is the highest operating frequency ($= 10.6$ GHz). The width w_{f1} of the 50-ohm microstrip transmission line was calculated by using the relationship between the characteristic impedance and the width for the microstrip transmission line [35]. Other design parameters of the reference LTSA were optimized to achieve the best impedance matching with wider bandwidth.

When hook-shaped slots were appended to the ground plane, as shown in Figure 2(b), the lower limit of the frequency band at a VSWR < 2 moved toward low frequency at around 2.97 GHz because of new resonance created by the hook-shaped slots [3]. The design parameters related to the hook-shaped slots were optimized through parameter sweep simulations. In this case, impedance matching deteriorated in the middle- and high-frequency regions from 7.31 GHz to 10.45 GHz. Therefore, the upper limit of the frequency band became 7.31 GHz, and the frequency bandwidth was reduced to 84.4%. Gain in the UWB increased to 2.8–6.0 dBi.

Next, a strip directorwas added, as shown in Figure 2(c), in order to increase gain in the middle- and high-frequency regions along with impedance matching enhancement. The dimensions of the strip director and the distance from the LTSA were optimized for the best impedance matching. The frequency band for a VSWR < 2 satisfied the UWB at 2.97 GHz to 11.76 GHz (119.4%). Gain was 3.0–7.6 dBi within the UWB. Gain increased by 0.2–1.6 dB in the 4 GHz to 10.6 GHz band, compared to Figure 2(b). The second director was placed about 3.4 mm above the first director, and the length of the second director was 6.2 mm with the same width of the first director.

After the second strip director was appended above the first strip director [3], as shown in Figure 2(d), the frequency band for a VSWR < 2 was almost the same as that of Figure 2(c), at 2.97 GHz to 11.77 GHz (119.4%). Gain was 3.1–7.8 dBi within the UWB. Gain increased by 0.1-0.5 dB in the 5.8 GHz to 11.2 GHz band, compared to Figure 2(c).

When two-layers of DS-MTMs were used instead of the two strip directors, as shown in Figure 2(e), impedance matching in the middle- and high-frequency regions from 8.42 GHz to 10.52 GHz was deteriorated, and the frequency band for a VSWR < 2 was reduced in the range from 2.96 GHz to

8.42 GHz (96.0%). Gain was 3.1–7.1 dBi within the UWB. We note that gain in the low- and middle-frequency regions is similar or slightly increased, compared to the previous cases, but it decreased in the high-frequency region at 9 GHz to 11 GHz.

Finally, when the proposed combined director consisting of an array of DS-MTM surrounding the first strip director was applied, as shown in Figure 2(f), gain in almost the whole UWB from 3.1 GHz to 9.9 GHz increased by 0.1–0.6 dB. The frequency band for a VSWR < 2 was slightly decreased to 2.97 GHz to 11.64 GHz (118.7%), whereas gain in the UWB was 3.3–7.4 dBi. Therefore, we can conclude that the gain enhancement effect from the surrounding DS-MTM arrays is better than that of the second strip director or the director using two-layer DS-MTM only.

Figure 4 compares the scattering parameters, effective refractive index, effective relative permittivity, effective relative permeability, and dispersion diagram of the single-sided (SS) MTM and DS-MTM. Note that eight thin strips are printed only on the top side of the substrate for the SS-MTM, whereas they are printed on both sides of the substrate for the DS-MTM. Perfect electric conductor (PEC) and perfect magnetic conductor (PMC) boundary conditions are employed to simulate the unit cell of the two MTMs and to obtain the scattering parameters. The effective parameters can be extracted from the scattering parameters [36]. We can see that the real parts of the effective refractive index and effective relative permittivity for the SS-MTM and DS-MTM are larger than those of the reference substrate without the eight thin strips. The real part of the effective relative permittivity ranges from 2.16 to 2.51 for DS-MTM, whereas it ranges from 1.85 to 2.17 for SS-MTM. It ranges from 1.14 to 1.24 for the reference substrate. Therefore, the real part of the effective relative permittivity of the SS-MTM and DS-MTM is larger than that of the reference substrate. Since higher dielectric materials are more effective to enhance gain of antennas when they are used as a lens or a director, we can expect that the gain enhancement effect in the DS-MTM would be betterthan the SS-MTM.

This trend can also be confirmed through the dispersion diagram. Figure 4(e) shows the dispersion diagram of the two MTMs. It was simulated using an eigen-mode solver in CST Studio Suite. The dominant modes for the unit cells of the SS- and DS-MTM lie below the light line in the slow wave region, and the MTMs have an effect of dielectric lens with a strong confinement of waves. In addition, the resonant or cut-off frequency of the DS-MTM is lower than that of the SS-MTM, with more slow wave effect through higher effective relative permittivity.

In order to understand the behaviors of the six antennas in more detail, the radiation patterns and electric-field distributions of the six antennas at 3.1 GHz, 6 GHz, and 9 GHz are compared in Figures 5 and 6. In the low-frequency region of 3.1 GHz, electric-fields were distributed in the tapered slot and all the edges of the surrounding ground plane for the reference LTSA. When the hook-shaped slots were inserted to the two side edges of the ground plane, the metallic part of the ground plane below the hook-shaped slots acted like a reflector, and electric-field distributions were concentrated on the hook-shaped slots. Gain of the antennas in Figures 2(b) to 2(f) was increased from 3.51 dBi to 3.64 dBi, compared to 1.13 dBi of the reference LTSA. In this case, there is not much difference in gain enhancement among the LTSAs with different types of directors.

Next, at the middle frequency region of 6 GHz, electric-fields were mainly distributed in the tapered slot and upper edges of the surrounding ground plane for the reference LTSA. When different types of directors were appended above the taper slot, electric fields were spread on the director region, and gain enhancement became larger. In addition, electric-field concentration on the upper region above the tapered slot was the highest for the proposed LTSA.

This resulted in the highest gain enhancement among the four antenna configurations with different director types, as shown in Figures 2(c) to 2(f). Gain of the antennas in Figures 2(b) to 2(f) at 6 GHz was increased from 3.43 dBi to 4.36 dBi, compared to 2.32 dBi of the reference LTSA. In addition, front-to-back (F/B) ratio was also increased from 7.21 dB to 10.95 dB, compared to 5.78 dB of the reference LTSA.

It is well known that LTSA acts as a traveling wave antenna in the high frequency region [14]. It has multiple wavelengths and multiple radiation regions with phase reversal along the tapered slot. This results in increased side lobes. As shown in Figure 6(c), in the high frequency region of 9 GHz, electric-fields were more distributed in the center regions of the tapered slot and upper edges of the surrounding ground plane for the reference LTSA, due to the multiple wavelengths along the tapered slot. In particular, it can be seen that side lobes in the H-plane increased for the antennas in Figures 2(c)

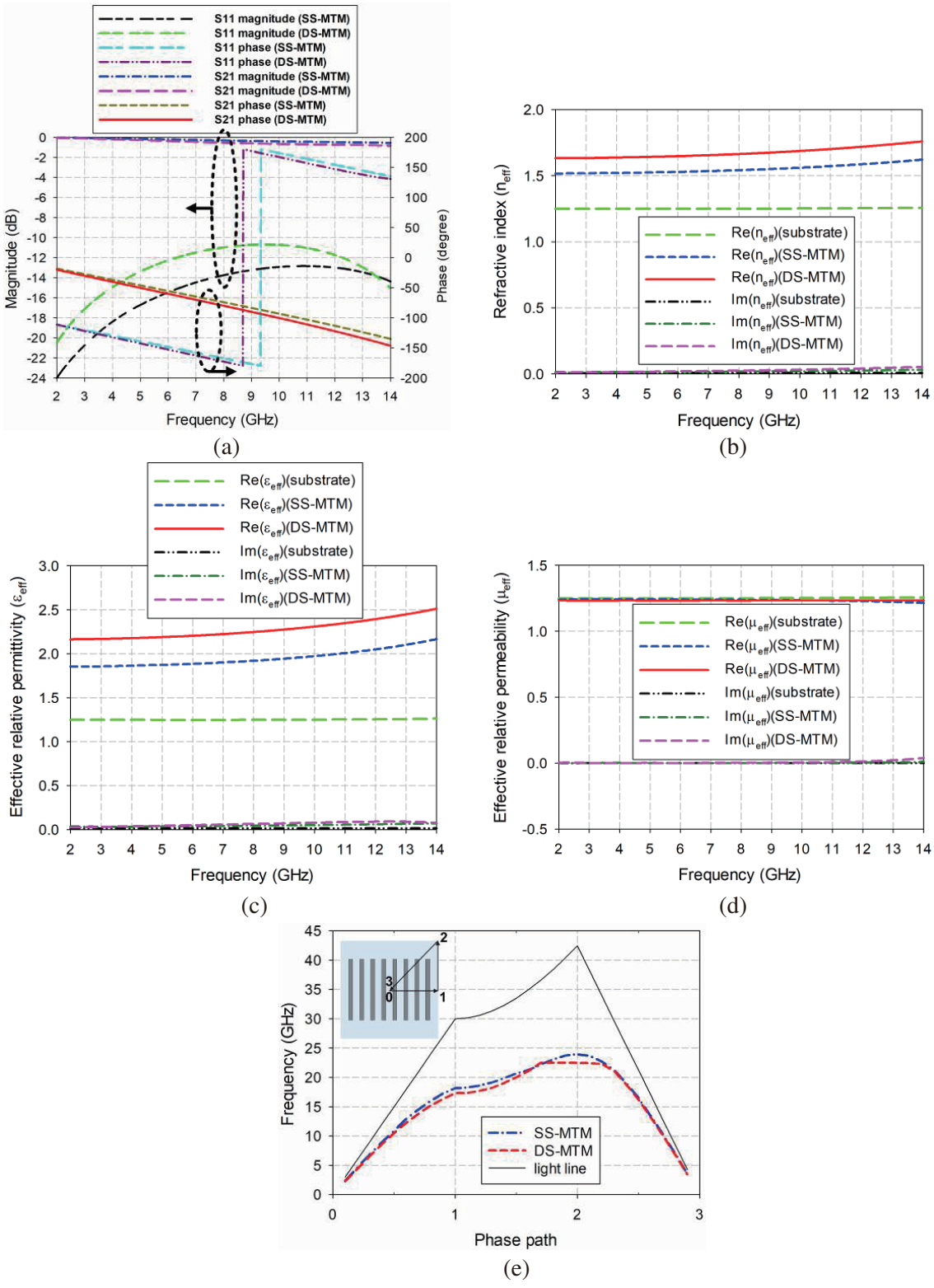

Figure 4. Comparison of scattering parameters, extracted parameters and dispersion diagram for SS- and DS-MTM: (a) scattering parameters, (b) effective refractive index, (c) effective relative permittivity, (d) effective relative permeability, and (e) dispersion diagram.

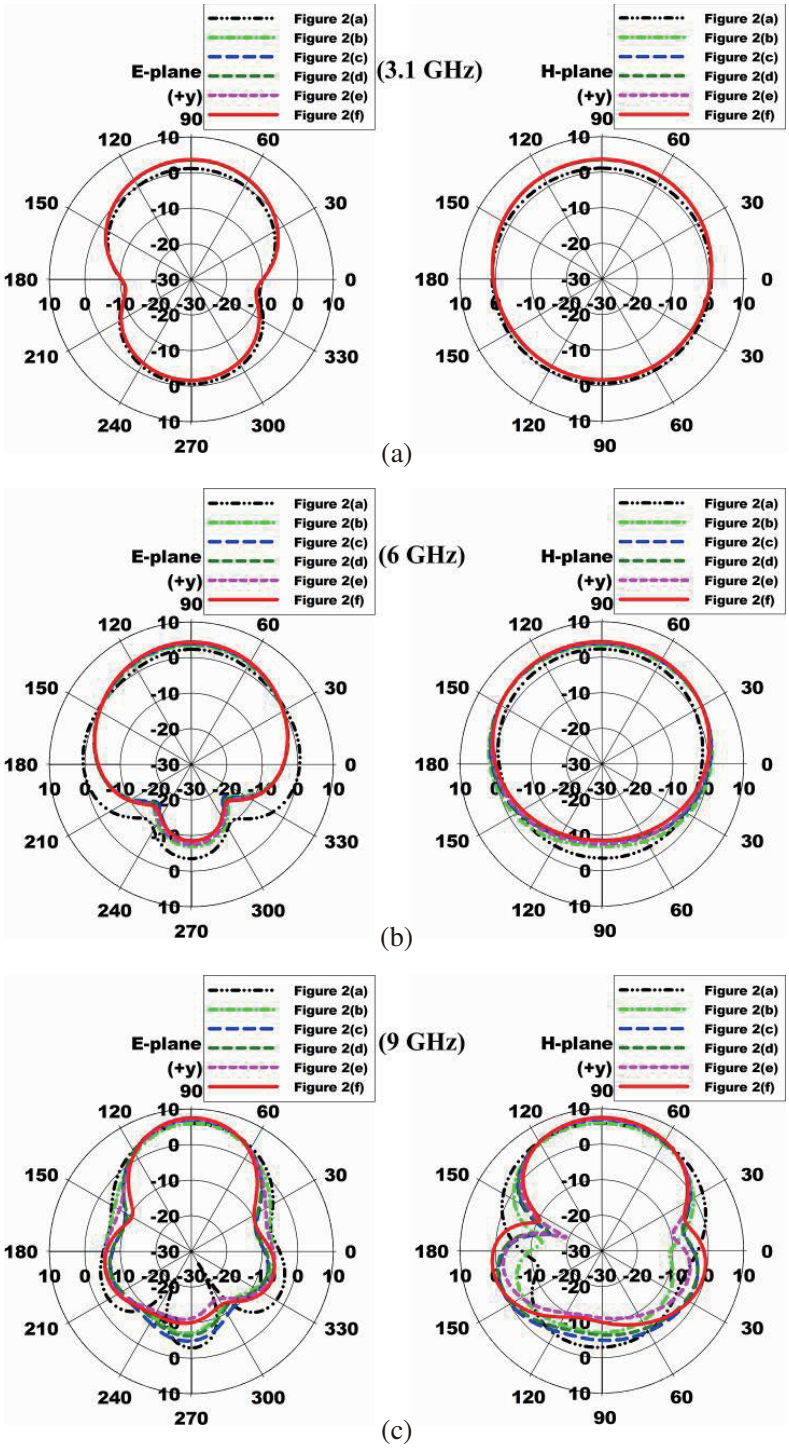

Figure 5. Comparison of radiation patterns for the antennas in Figure 2 at (a) 3.1 GHz, (b) 6 GHz, and (c) 9 GHz.

to 2(f). This might be caused by the interaction between various types of directors and the upper edges of the ground plane. For the proposed LTSA, side lobe levels along the horizontal direction might be further increased due to the field interaction between the DS-MTM and the upper edges of the ground plane [37]. Gain of the antennas in Figures 2(b) to 2(f) was increased from 5.97 dBi

to 7.48 dBi, compared to 5.91 dBi of the reference LTSA. F/B ratio was increased from 11.67 dB to 18.07 dB, compared to 9.0 dB of the reference LTSA.

Simulated surface current distributions of the proposed LTSA are shown in Figure 7 at 3.1 GHz, 6 GHz, and 9 GHz. The surface currents at 3.1 GHz are mainly distributed on the hook-shaped slots, whereas those on the conductors between the tapered slot and hook-shaped slots and the strip director are enhanced at 6 GHz. At 9 GHz, the surface currents are concentrated on the conductors between the tapered slot and hook-shaped slots and the combined director.

3. EXPERIMENT RESULTS AND DISCUSSION

Figures 8(a) and (b) show the fabricated prototype of the proposed compact LTSA. An Agilent N5230A network analyzer is used to measure the performance of the fabricated antenna in an anechoic chamber. Standard one-port SOL(Short-Open-Load) calibration was used for the input reflection coefficient

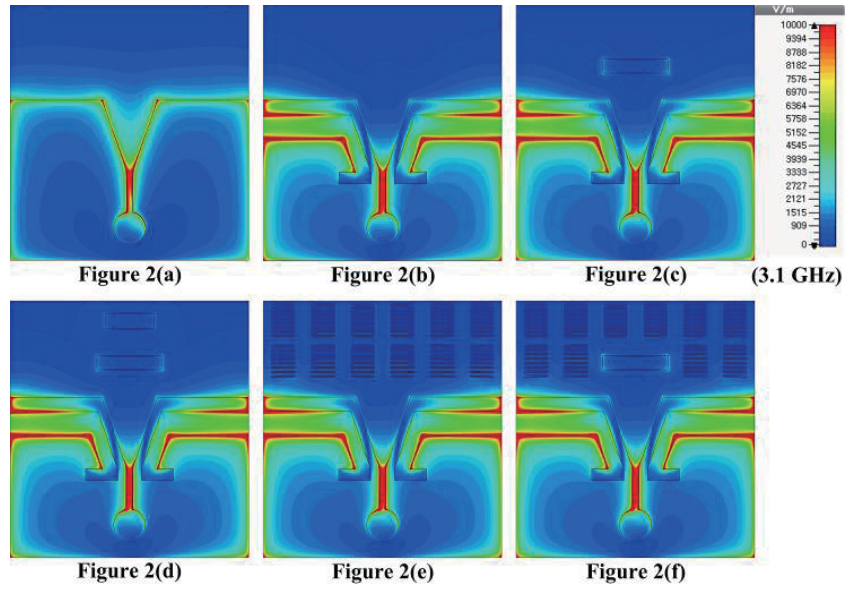

(a)

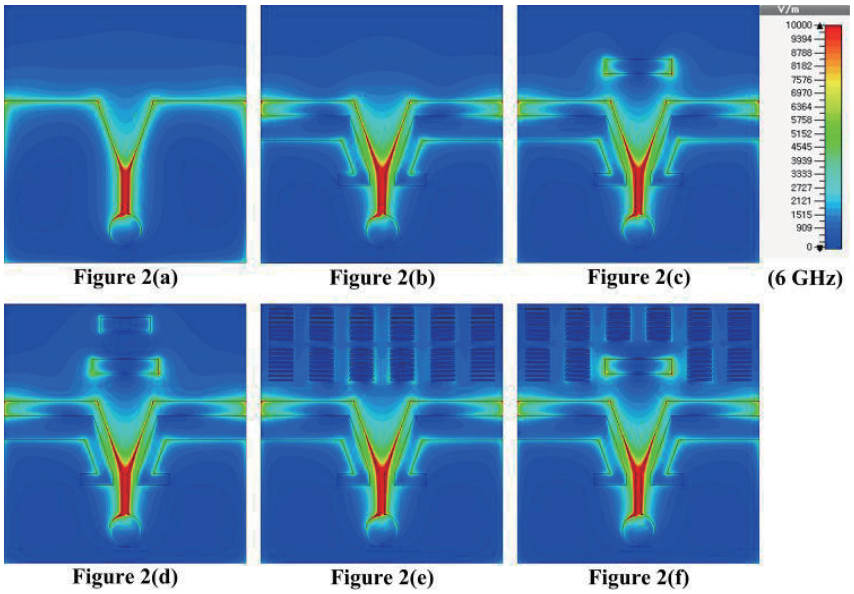

(b)

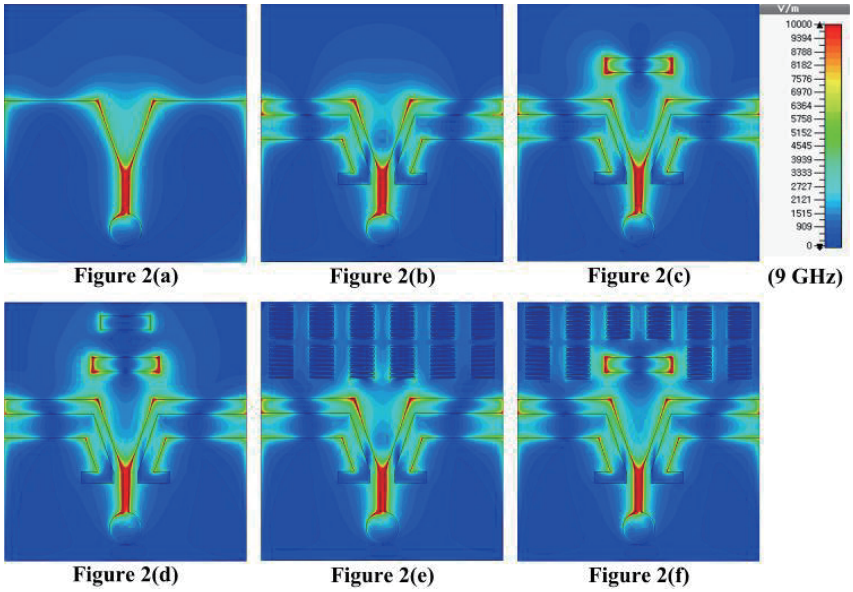

Figure 6. Electric field distributions comparison for the antennas in Figure 2 at (a) 3.1 GHz, (b) 6 GHz, and (c) 9 GHz.

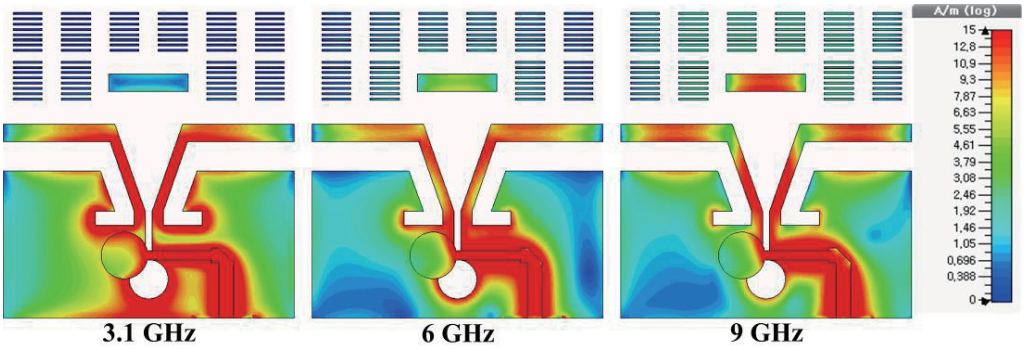

Figure 7. Surface current distributions of the proposed LTSA at 3.1 GHz, 6 GHz, and 9 GHz.

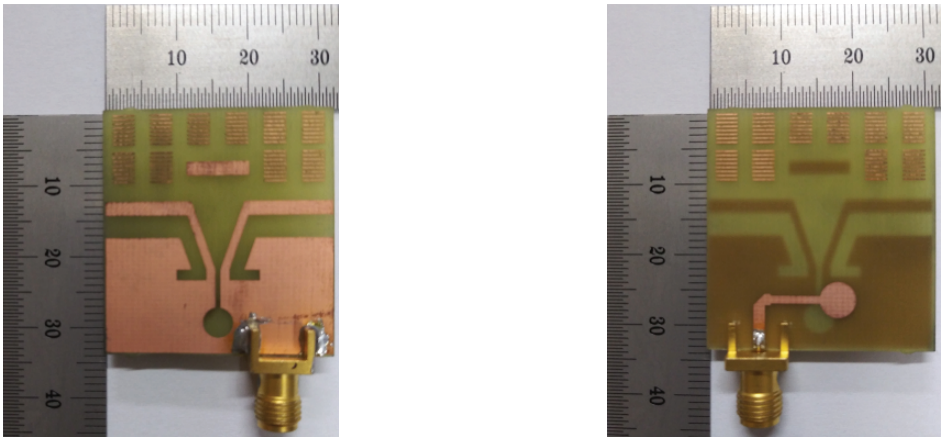

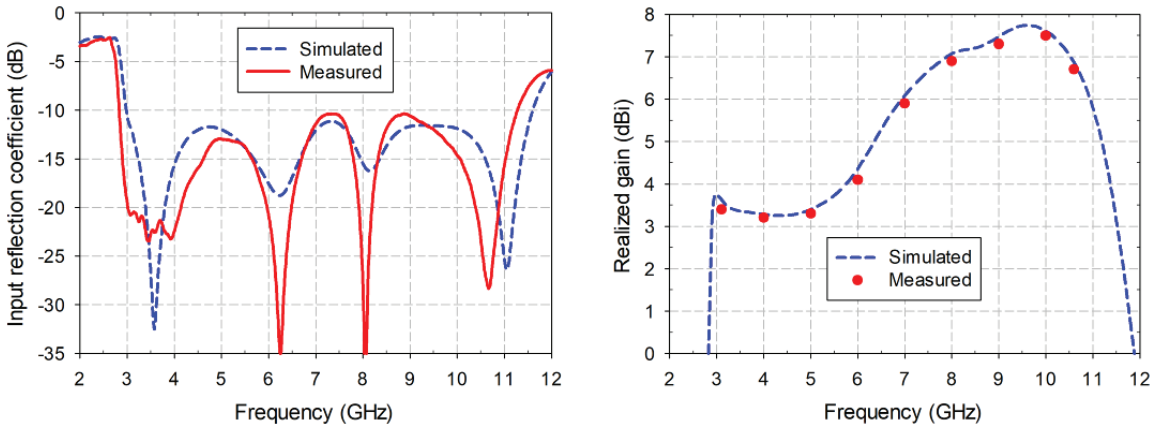

(c) (d)

Figure 8. Photographs and performances of the fabricated antenna, (a) front view, (b) back view, (c) input reflection coefficient, and (d) realized gain.

measurement. The measured results are compared with the simulation in Figures 8(c) and 8(d). The measured frequency band for a VSWR < 2 is 2.83 GHz to 11.31 GHz (119.9%). Both lower and higher frequency limits shift slightly towards the lower frequency, compared to the simulated result. The measured peak gain is 3.2–7.5 dBi, which decreased slightly compared to the simulation. The difference between the measured and simulated results might be caused by measurement setup and/or manufacturing error.

Figure 9 shows the measured radiation patterns of the fabricated antenna on the x-y and y-z planes. The measured radiation patterns agree well with the simulated results for both planes. The measured front-to-back ratio of the proposed LTSA is larger than 8.1 dB with directional beam patterns.

Measured group delay of the fabricated antenna is shown in Figure 10. Two proposed antennas face each other along the main beam direction for the measurement with a separate distance of 300 mm. The variation of the proposed antenna in the frequency range of 3 GHz to 11 GHz is less than ± 0.5 ns. Therefore, it can be said that the time domain characteristic of the proposed antenna is good to be used as a UWB antenna.

The dimensions and performance of the proposed compact LTSA are compared in Table 2 with other compact UWB TSAs described in introduction. We can see that the dimensions of the proposed LTSA are the smallest among the antennas in Table 2 with moderate gain over 3.2 dBi in the operating band.

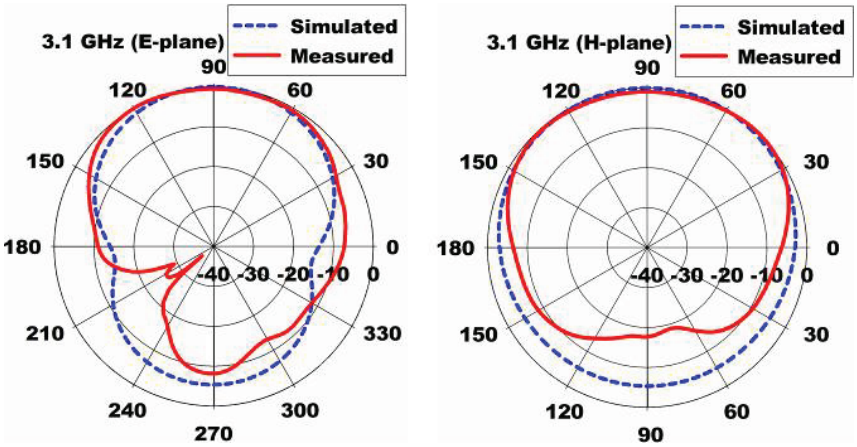

(a)

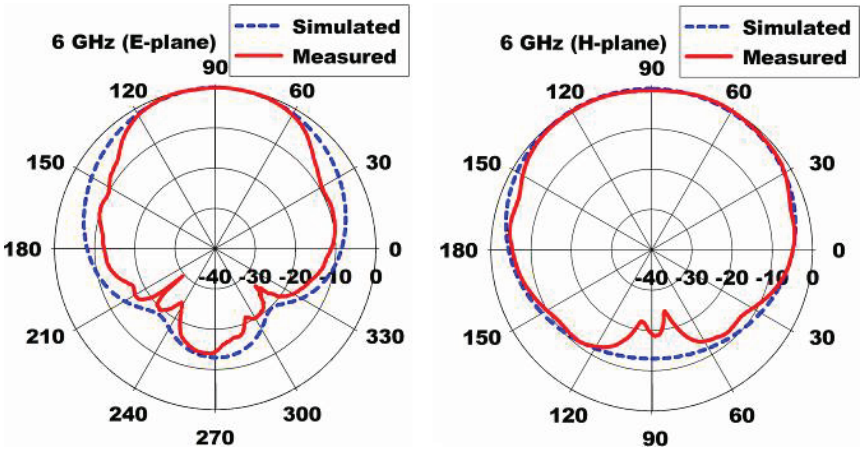

(b)

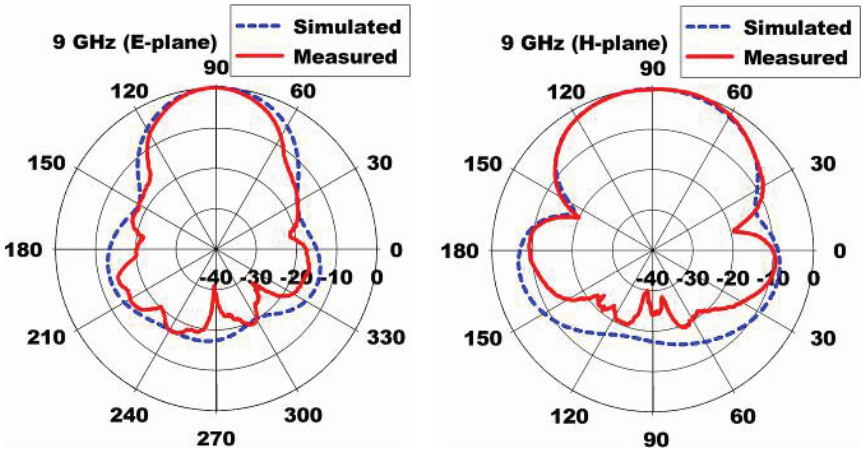

(c)

Figure 9. Measured radiation patterns at (a) 3.1 GHz, (b) 6 GHz, and (c) 9 GHz.

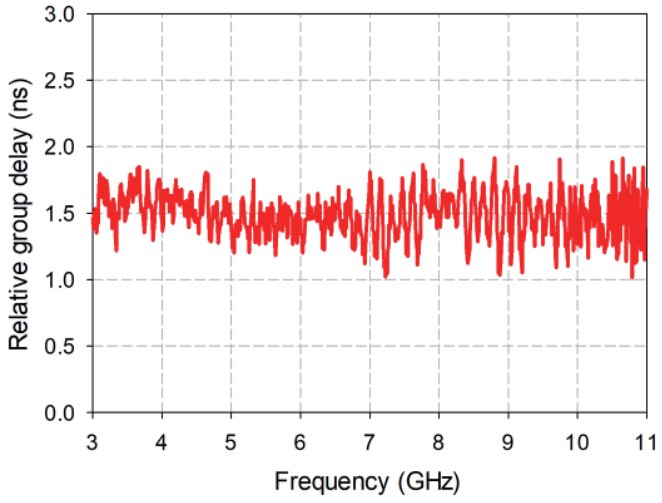

Figure 10. Measured group delay of the fabricated antenna.

Table 2. Comparison of dimensions, and performance of the proposed LTSA with other compact UWB LTSAs in the literature.

	Physical sizes (mm^3)	Electrical sizes (λ_0^3)	Bandwidth (GHz)	Gain (dBi)
[7]	$35 \times 36 \times 0.8$	$0.36 \times 0.37 \times 0.0083$	3.10–11.00 (112.0%)	2.0–8.0
[8]	$37 \times 34 \times 0.8$	$0.39 \times 0.36 \times 0.0085$	3.20–10.50 (106.6%)	1.5–8.1
[9]	$36 \times 36 \times 0.8$	$0.36 \times 0.36 \times 0.0080$	3.00–12.80 (124.1%)	3.7–8.3
[10]	$36 \times 32 \times 2.0$	$0.30 \times 0.26 \times 0.0200$	2.50–11.00 (125.9%)	3.4–8.4
[11]	$45 \times 40 \times 0.8$	$0.44 \times 0.39 \times 0.0079$	2.96–5.05/ 5.58–8.52(96.9%)	2.6–7.0
[12]	$158 \times 125 \times 1.0$	$0.44 \times 0.39 \times 0.0024$	0.72–17 (183.8%)	1–12.5
[13]	$42.9 \times 29.3 \times 0.81$	$0.38 \times 0.30 \times 0.0081$	3.00–13.48 (127.2%)	2.2–6.5
[15]	$40 \times 40 \times 1.6$	$0.33 \times 0.33 \times 0.0133$	2.5–11 (125.9%)	−1.5–7.2
[17]	$50 \times 52.5 \times 0.762$	$0.33 \times 0.35 \times 0.0051$	2–18.7 (161.4%)	0–10.5
[20]	$96 \times 140 \times 0.508$	$0.32 \times 0.47 \times 0.0017$	1–30 (187.1%)	2.2–11
[26]	$42 \times 45 \times 0.8$	$0.43 \times 0.47 \times 0.0083$	3.1–12 (117.9%)	1–8.3
[28]	$80 \times 150 \times 1.0$	$0.30 \times 0.57 \times 0.0038$	1.13–12 (165.6%)	1–10.5
This work	$30 \times 32 \times 0.8$	$0.28 \times 0.30 \times 0.0075$	2.83–11.31 (119.9%)	3.2–7.5

4. CONCLUSION

In this paper, in order to design a compact gain-enhanced LTSA for UWB applications, hook-shaped slots in the ground plane and a combined director above the tapered slot, consisting of a strip director and DS-MTM loading surrounding it, have been employed. It was demonstrated that the proposed combined director shows better gain enhancement than other director configurations, such as single strip director, two strip directors, and two-layers of DS-MTMs. In addition, the size of the proposed LTSA with a combined director is smaller than the other compact TSAs in the literature.

The fabricated prototype of the proposed antenna provided a frequency band of 2.83 GHz to 11.31 GHz (119.9%) for a VSWR < 2 with UWB gain of 3.2–7.5 dBi.

The proposed compact, gain-enhanced LTSA can be used as a compact directional antenna for retransmission-based UWB chipless RFID tags or other UWB communication applications.

REFERENCES

1. Federal Communications Commission, Washington, DC, "FCC report and order on ultra wideband technology," 2002.

2. Schantz, H., *The Art and Science of Ultrawideband Antennas*, Artech House, Norwood, 2005.
3. Yeo, J., "Miniaturized UWB stepped open-slot antenna," *Progress In Electromagnetics Research Letters*, Vol. 78, 119–127, 2018.
4. Eberle, J., C. Levis, and D. McCoy, "The flared slot: A moderately directive flush-mounted broadband antenna," *IRE Trans. Antennas Propag.*, Vol. 8, No. 5, 461–468, Sep. 1960.
5. Gibson, P. J., "The Vivaldi aerial," *Proc. 9th Eu. Microw. Conf.*, Vol. 1, 101–105, 1979.
6. Abbosh, A., M. Bialkowski, and H. Kan, "Planar tapered slot antennas," *Printed Antennas for Wireless Communications*, 1st Edition, Ch. 6, 161–162, John Wiley & Sons, Hoboken, NJ, 2007.
7. Zhu, F., S. Gao, A. T. S. Ho, C. H. See, R. A. Abd-Alhameed, J. Li, and J. Xu, "Compact-size linearly tapered slot antenna for portable ultra-wideband imaging systems," *Int. J. RF Microwave Comput. — Aided Eng.*, Vol. 23, No. 3, 290–299, Aug. 2012.
8. Zhu, F. and S. Gao, "Compact elliptically tapered slot antenna with nonuniform corrugations for ultra-wideband applications," *Radioengineering*, Vol. 22, No. 1, 276–280, Apr. 2013.
9. Ma, K., Z. Zhao, J. Wu, S. M. Ellis, and Z. P. Nie, "A printed Vivaldi antenna with improved radiation patterns by using two pairs of eye-shaped slots for UWB applications," *Progress In Electromagnetics Research*, Vol. 148, 63–71, 2014.
10. Yang, D., S. Liu, and D. Geng, "A miniaturized ultra-wideband Vivaldi antenna with low cross polarization," *IEEE Access*, Vol. 5, 23352–23357, 2017.
11. Seo, J., J. H. Kim, and J. Oh, "Semicircular patch-embedded Vivaldi antenna for miniaturized UWB radar sensors," *Sensors*, Vol. 20, 5988, 2020.
12. Honari, M. M., M. S. Ghaffarian, and R. Mirzavand, "Miniaturized antipodal Vivaldi antenna with improved bandwidth using exponential strip arms," *Electronics*, Vol. 10, 83, 2021.
13. Saleh, S., W. Ismail, I. S. Z. Abidin, M. H. Jamaluddin, M. H. Bataineh, and A. S. Alzoubi, "Compact UWB Vivaldi tapered slot antenna," *Alex. Eng J.*, Vol. 61, No. 6, 4977–4994, Jun. 2022.
14. Nassar, I. T. and T. M. Weller, "A novel method for improving antipodal Vivaldi antenna performance," *IEEE Trans. Antennas Propag.*, Vol. 63, No. 7, 3321–3324, Jul. 2015.
15. Samsuzzaman, M., M. T. Islam, A. A. S. Shovon, R. I. Faruque, and N. Misran, "A 16-modified antipodal Vivaldi antenna array for microwave-based breast tumor imaging applications," *Microw. Opt. Technol. Lett.*, Vol. 61, No. 9, 2110–2118, Jun. 2019.
16. Li, Z., X. Kang, J. Su, Q. Guo, Y. Yang, and J. Wang, "A wideband end-fire conformal Vivaldi antenna array mounted on a dielectric cone," *Int. J. Antennas Propag.*, Vol. 2016, Art. No. 9812642, Aug. 2016.
17. Gao, C., E. Li, Y. Zhang, and G. Guo, "A directivity enhanced structure for the Vivaldi antenna using coupling patches," *Microw. Opt. Technol. Lett.*, Vol. 60, No. 2, 418–424, Jan. 2018.
18. Bourqui, J., M. Okoniewski, and E. C. Fear, "Balanced antipodal Vivaldi antenna with dielectric director for near-field microwave imaging," *IEEE Trans. Antennas Propag.*, Vol. 58, No. 7, 2318–2326, Jul. 2010.
19. Molaei, A., M. Kaboli, M. S. Abrishamian, and S. A. Mirtaheri, "Dielectric lens balanced antipodal Vivaldi antenna with low cross-polarisation for ultra-wideband applications," *IET Microw., Antennas Propag.*, Vol. 8, No. 14, 1137–1142, Nov. 2014.
20. Moosazadeh, M., S. Kharkovsky, J. T. Case, and B. Samali, "Miniaturized UWB antipodal Vivaldi antenna and its application for detection of void inside concrete specimens," *IEEE Antennas Wireless Propag. Lett.*, Vol. 16, 1317–1320, 2017.
21. Moosazadeh, M. and S. Kharkovsky, "A compact high-gain and front-to-back ratio elliptically tapered antipodal Vivaldi antenna with trapezoid-shaped dielectric lens," *IEEE Antennas Wireless Propag. Lett.*, Vol. 15, 552–555, 2016.
22. Amiri, M., F. Tofigh, A. Ghafoorzadeh-Yazdi, and M. Abolhasan, "Exponential antipodal Vivaldi antenna with exponential dielectric lens," *IEEE Antennas Wireless Propag. Lett.*, Vol. 16, 1792–1795, 2017.

23. Huang, D., H. Yang, Y. Wu, F. Zhao, and X. Liu, "A high-gain antipodal Vivaldi antenna with multi-layer planar dielectric lens," *Journal of Electromagnetic Waves and Applications*, Vol. 32, No. 4, 403–412, Oct. 2017.
24. Li, X. X., D. W. Pang, H. L. Wang, Y. M. Zhang, and G. Q. Lv, "Dielectric slabs covered broadband Vivaldi antenna for gain enhancement," *Progress In Electromagnetics Research C*, Vol. 77, 69–80, 2017.
25. Zhou, B. and T. J. Cui, "Directivity enhancement to Vivaldi antennas using compactly anisotropic zero-index metamaterials," *IEEE Antennas Wireless Propag. Lett.*, Vol. 10, 326–329, 2011.
26. Pandey, G. K., H. S. Singh, and M. K. Meshram, "Meander-line-based inhomogeneous anisotropic artificial material for gain enhancement of UWB Vivaldi antenna," *Appl. Phys. A*, Vol. 122, 134, 2016.
27. Boujemaa, M.-A., R. Herzi, F. Choubani, and A. Gharsallah, "UWB antipodal Vivaldi antenna with higher radiation performances using metamaterials," *Appl. Phys. A*, Vol. 124, No. 10, 714, 1–7, Sep. 2018.
28. Zhu, S., H. Liu, P. Wen, L. Du, and J. Zhou, "A miniaturized and high gain double-slot Vivaldi antenna using wideband index-near-zero metasurface," *IEEE Access*, Vol. 6, 72015–72024, 2018.
29. Islam, M. T., M. Samsuzzaman, S. Kibria, N. Misran, and M. T. Islam, "Metasurface loaded high gain antenna based microwave imaging using iteratively corrected delay multiply and sum algorithm," *Sci. Rep.*, Vol. 9, 17317, 2019.
30. Chen, L., Z. Lei, R. Yang, J. Fan, and X. Shi, "A broadband artificial material for gain enhancement of antipodal tapered slot antenna," *IEEE Trans. Antennas Propag.*, Vol. 63, No. 1, 395–400, Jan. 2015.
31. Li, X., G. Liu, Y. Zhang, L. Sang, and G. Lv, "A compact multi-layer phase correcting lens to improve directive radiation of Vivaldi antenna," *Int. J. RF Microw. Comput. — Aided Eng.*, Vol. 27, No. 7, Apr. 2017.
32. Li, X., H. Zhou, Z. Gao, H. Wang, and G. Lv, "Metamaterial slabs covered UWB antipodal Vivaldi antenna," *IEEE Antennas Wireless Propag. Lett.*, Vol. 16, 2943–2946, 2017.
33. Electromagnetic Simulation Solvers, CST Studio Suite, Available online: https://www.3ds.com/ko/products-services/simulia/products/cst-studio-suite/solvers/ (accessed on 23 November 2022).
34. Tseng V. and C. Y. Chang, "Linear tapered slot antenna for ultra-wideband radar sensor: design consideration and recommendation," *Sensors*, Vol. 19, No. 5, 1212, 2019.
35. Huang Y. and K. Boyle, *Antennas: From Theory to Practice*, John Wiley & Sons, Inc., Hoboken, NJ, 2008.
36. Szabó, Z., G. Park, R. Hedge, and E. Li, "A unique extraction of metamaterial parameters based on Kramers-Kronig relationship," *IEEE Trans. Microw. Theory Techn.*, Vol. 58, No. 10, 2646–2653, Oct. 2010.
37. Ma, X., M. S. Mirmoosa, and S. A. Tretyakov, "Parallel-plate waveguides formed by penetrable metasurfaces," *IEEE Trans. Antennas Propag.*, Vol. 68, No. 3, 1773–1785, Mar. 2020.